RSC Advances

PAPER

Cite this: *RSC Adv.*, 2020, **10**, 26451

Preparation of low carbon olefins on a core–shell K–Fe_5C_2@ZSM-5 catalyst by Fischer–Tropsch synthesis

Yang Liu,[a] Wenli Shao,[a] Yi Zheng,[a] Chenyang Zhang,[a] Weixia Zhou,[a] Xueqin Zhang *[a] and Yongjun Liu *[ab]

In this study, a core–shell catalyst based on Fe_5C_2@ZSM-5 (ZSM-5 capped Fe_5C_2 as active phase) is prepared by the coating-carbonization method for Fischer–Tropsch synthesis (FTS). Further, the designed ZSM-5 zeolites are utilized to screen the low carbon hydrocarbons from the products generated on the iron carbide active centre, and for catalytic disassembly of the long-chain hydrocarbons into low carbon olefins. Prior to utilization, the physical–chemical properties of the prepared catalysts are systematically characterized by various techniques of X-ray diffraction (XRD), Brunauer–Emmett–Teller (BET), Fourier transform infrared (FT-IR), and scanning electron microscopy (SEM) as well as transmission electron microscopy (TEM) observations, in addition to the effects of coating-carbonization, molecular sieve coating amount, and K-doping on core–shell iron-based catalysts. Next, the performance of Fischer–Tropsch synthesis is investigated in a micro-fixed bed reactor. The results manifest that, comparing with Fe_5C_2 and a supported Fe/ZSM-5 catalyst prepared by the traditional impregnation method, the core–shell Fe_5C_2@ZSM-5 catalysts show higher CO conversion rate, reaction activity and selectivity to low-carbon olefins. Comparatively, the Fe_5C_2@ZSM-5C catalyst prepared by carbonization after the coating method exhibited more surface area, smaller average pore size, and more reactive active sites, resulting in the improvement of screening of high carbon hydrocarbons and the enhancement of selectivity to low carbon olefins, in comparison to those prepared by the carbonization-coating method. In conclusion, the K-doping catalyst had significantly improved the reactive activity of the core–shell Fe_5C_2@ZSM-5 catalyst and the selectivity to low carbon olefins, while the CO conversion on K–Fe_5C_2@ZSM-20C still remained good.

Received 5th April 2020
Accepted 2nd July 2020

DOI: 10.1039/d0ra03074k

rsc.li/rsc-advances

Introduction

With the increasing exhaustion of fossil energy and the rapid increase in energy demand, it is required to find an alternative to replacing fossil energy. As a substitute, Fischer–Tropsch synthesis (FTS), a feasible gas-to-liquids technology for the production of clean transportation fuels and building-block chemicals from non-petroleum carbon resources, was first reported by German scientists Han Fischer and Franz Tropsch in 1923.[1,2] FTS reaction mainly refers to the heterogeneous hydrogenation reaction of CO and H_2 as raw materials under the action of catalyst (iron-based and cobalt-based catalysts), resulting in the major products of alkanes and olefins with a wide carbon number distribution.[3–5] In addition, this approach results in several by-products such as alcohol, ketone, aldehyde, acid, or ester.[6] Amongst them, the low carbon olefins, such as ethylene and propylene, are highly regarded as extensive and prosperous platform chemical compounds. It should be noted that the key factor that plays a crucial role in producing low carbon olefins in the FTS is the highly active and selective catalyst.[7,8] To address this aspect, the iron-based catalysts have been widely used as one of the most important kinds of industrial catalysts for FTS reactions.[9] However, the conventional iron-based catalysts often suffer from various disadvantages such as wide carbon number distribution, high methane or oxygen-containing organic matter, the high proportion of high-carbon linear alkane in the products, and easy inactivation at high temperature.[10] Interestingly, some of the reports concluded that the selectivity of lower carbon olefins could be improved by breaching the undesired high carbon number linear alkane in the products. In addition, high temperature (300–350 °C) on the FTS reaction is beneficial to the formation and selectivity of low carbon olefins.[11] Therefore, it is highly required to develop an FTS catalyst, which is resistant to high temperatures and has a high selectivity of low-carbon olefins is recommended.

[a]*College of Chemical Engineering, Huaqiao University, Xiamen 361021, P. R. China. E-mail: xqzhang2009@hqu.edu.cn; yongjunliu@hqu.edu.cn*

[b]*Institution of Chemical Process and Intrinsic Safety, Huaqiao University, Xiamen 361021, P. R. China*

Indeed, various reports have demonstrated that iron carbide is the ultimate active phase of iron-based catalyst for FTS reaction,[12–16] providing an active iron center for CO hydrogenation.[17] However, the currently available iron-based catalysts are mostly based on iron oxide as the main active component.[13,18–20] During the FTS reaction, the active phase of iron carbide is gradually formed *via* carbonization of iron oxide by CO, resulting in a reactive active phase with an unstable structure. It should be noted that such an unstable structure not only reduces the activity of the FTS reaction of the iron-based catalyst but also increases the difficulty of the reaction process.[21] Therefore, the direct utilization of iron carbide as the active phase of CO hydrogenation in this research is recommended.

Further, the addition of the alkali promoter is an effective method for enhancing the catalytic activity and selectivity of olefins in products. Previous reports indicated that the addition of alkali metal to Fe-based catalysts could help to reduce the electron affinity of iron and the adsorption capacity for H_2,[22] thereby reducing the hydrogenation activity of CO, enhancing the adsorption capacity of CO, and changing the selectivity of products. In addition, molecular sieve carriers offer the advantages of uniform and controllable pore structure and adjustable acidity, which can play the role of screening and catalytic cracking.[23–25] Therefore, we combined the molecular sieve with iron carbide, taking iron carbide as the core and ZSM-5 molecular sieve as the shell, resulting in the core–shell Fe_5C_2@ZSM-5 catalysts.

In this work, the core–shell Fe_5C_2@ZSM-5 catalysts were modified by changing the coating amount of molecular sieve and adding a K^+ promoter. Then, we investigated the performance of the core–shell K–Fe_5C_2@ZSM-5 catalysts on FTS reaction and compared with the supported K–Fe/ZSM-5 catalyst that was prepared by a traditional impregnation method.

Experimental

Materials

Iron(III) nitrate nonahydrate (AR), deionized water, aluminum isopropoxide (CP), isopropanol (AR), ethyl alcohol absolute (AR), potassium nitrate (AR), copper(II) nitrate hydrate (AR), manganese nitrate (AR), and ZSM-5 were obtained from Sinopharm Chemical Reagent Co., Ltd., (Shanghai, China). Ammonium hydroxide (AR) and nitric acid (GR) were achieved from Xilong Scientific Co., Ltd. (Guangdong, China).

Synthesis of catalyst

The core–shell Fe_5C_2@ZSM-5 catalysts were prepared with different orders of coating and carbonization. While the coating amount of ZSM-5 molecular sieve was 30 wt%, the catalyst prepared by coating after carbonization was recorded as Fe_5C_2@ZSM-5-30, and the catalyst prepared by carbonization after coating was recorded as Fe_5C_2@ZSM-5-30C. Other logograms were similar.

Preparation of the precursor of Fe_5C_2

An appropriate amount of $Fe(NO_3)_3 \cdot 9H_2O$ was dissolved in 30 ml of water and stirred for 30 min. Then, ammonia was added dropwise to the solution, and the pH was adjusted to 10. Further, the solution was left overnight, drained, and washed the filter cake with deionized water until the pH of the filtrate reached 7. The filter cake was then placed in the oven and dried at 120 °C for about 12 h. Finally, the filter cake was ground for use to obtain Fe_2O_3, the precursor of Fe_5C_2.

Preparation of boehmite sol

Accurately weighed 41 g of aluminum isopropoxide, and 60 g of isopropanol were mixed in a 500 ml three-port flask and left still for 3 h at 50 °C. Then, 360 ml of deionized water was added slowly, stirred mechanically at 80 °C for 2 h, and heated to 90 °C. 9.45 ml of nitric acid at a concentration of 1.45 mol l^{-1} was added to the flask for reflux condensation for 10 h. Finally, the flask was placed in the air to evaporate some of the water and the unreacted isopropanol. The resultant white gel was denoted as boehmite sol, also known as ALOOH.

Preparation of core–shell Fe_2O_3@ZSM-5

The preparation process of core–shell Fe_2O_3@ZSM-5 is shown in Fig. 1. 20 ml anhydrous ethanol, 2 g boehmite sol, and the proper amount of ZSM-5 molecular sieve were mixed in a 100 ml beaker, and then stirred with the assistance of ultrasound for 2 h to obtain the uniform coating solution. The as-prepared solution was uniformly sprayed on the surface of Fe_2O_3 particles (iron carbide precursor). Further, the particles were dried at 80 °C for 12 h and roasted at 450 °C for 4 h in the oven to form the core–shell Fe_2O_3@ZSM-5.

Further, the particles of core–shell Fe_2O_3@ZSM-5 were loaded into a tubular furnace and calcined at 350 °C for 4 h in CO flow (200 ml min^{-1}) with the temperature ramp of 2.7 °C min^{-1}. The tubular furnace was finally cooled down naturally to room temperature and switched the gas CO to N_2 (100 ml min^{-1}). The prepared core–shell Fe_5C_2@ZSM-5 catalyst was sealed in N_2. For the preparation of the K-modified core–shell Fe_5C_2@ZSM-5 catalyst, a certain amount of KNO_3 was added into the solution of Fe_2O_3 precursor. All the experimental processes and parameters were followed, as stated above.

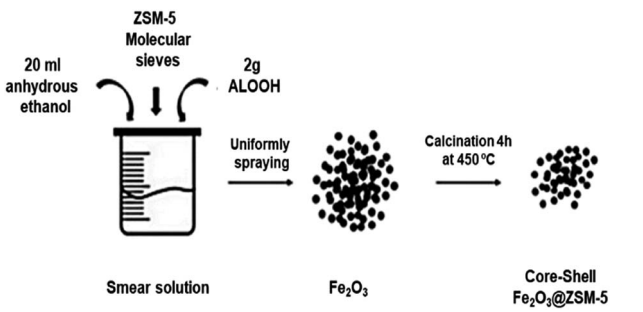

Fig. 1 Schematic showing the synthetic process of core–shell Fe_2O_3@ZSM-5.

Preparation of core–shell Fe_5C_2@ZSM-5 catalysts

Notably, two important steps in the preparation of the core–shell Fe_5C_2@ZSM-5 catalyst were followed. One of them was the uniform coating of ZSM-5 molecular sieve, while the other was the carbonization of Fe_2O_3. One of the preparing process, described here as an example, was carbonization after coating. In order to prevent the oxidation of Fe_5C_2, it was then quickly stored in paraffin and used for further experiments.

Preparation of supported K–Fe/ZSM-5 catalysts

Initially, accurately weighed 12.7311 g of $Fe(NO_3)_3 \cdot 9H_2O$ and 0.2549 g of KNO_3 were dispersed in 10 ml of deionized water to prepare a solution, such that the molar ratio of Fe : K was 25 : 2. Further, a certain amount of ZSM-5 was slowly added into the stated solution, and then stirred for 30 min and subjected to ultrasonication for 2 h. Then, the K–Fe/ZSM-5 precursors were placed in an oven at 80 °C for 12 h. Finally, the prepared particles were ground and calcined at 450 °C for 4 h in a resistance furnace to obtain the supported K–Fe/ZSM-5 catalysts.

Characterizations

As-prepared samples were characterized by X-ray diffraction (XRD, Rigaku, Tokyo, Japan), operated at 40 kV and 30 mA, and equipped with Cu-Kα radiation ($\lambda = 0.1542$ nm) in the 2θ range of 10–80° at a scanning rate of 10° min^{-1}. The specific surface area and pore size distribution of the designed catalyst samples were measured at 77.35 K on N_2-adsorption (Boynton Beach, FL, USA). The Brunauer–Emmett–Teller (BET) and Barrett–Joyner–Halenda (BJH) methods were used to obtain the specific surface area and the pore size distribution of the samples, respectively. To determine the chemical functionalities, Fourier transform infrared spectroscopy (FTIR) was employed using a SHIMADZUFT-IR-8400s (Kyoto, Japan). Prior to measurement, the sample was fully ground to 200 meshes and dried at 100 °C under vacuum. The mixture of sample and KBr were ground and pressed into a pellet and analysed using the spectrometer at the scanning range of 4000 to 400 cm^{-1}. The size, as well as the morphology of as-synthesized catalysts, were performed by scanning electron microscope (SEM, SU8000) and high-resolution transmission electron microscopy (HRTEM, H-7650). TEM images were obtained with an acceleration voltage of 120 kV.

Reactivity evaluation of FTS

The FTS reaction process was performed on a micro fixed bed catalytic reaction device. The flow chart of the apparatus for FTS is shown in Fig. 2. FTS reaction conditions were as follows: as-prepared catalysts weight of 100 mg; space velocity of 6000 ml h^{-1} g^{-1}; reaction temperature of 320 °C; reaction pressure of 1 MPa; and H_2/CO molar ratio of 2 : 1. The components of raw gas and tail gas were analysed by GS-TCD and GS-FID, respectively. GS-TCD was used to detect the contents of H_2, N_2, CH_4, CO, CO_2, while GC-FID was used to detect the contents of CH_4, C_2H_4, C_2H_6, C_3H_6, C_3H_8, C_4H_8, and C_4H_{10}.

The internal standard method was employed for data processing, N_2, and CH_4 as an internal standard for TCD and FID detection, respectively. The conversions of CO as C_{CO}, and the selectivity of CO_2 as S_{CO_2} and hydrocarbon as S_i (i: CH_4, C_2H_4,

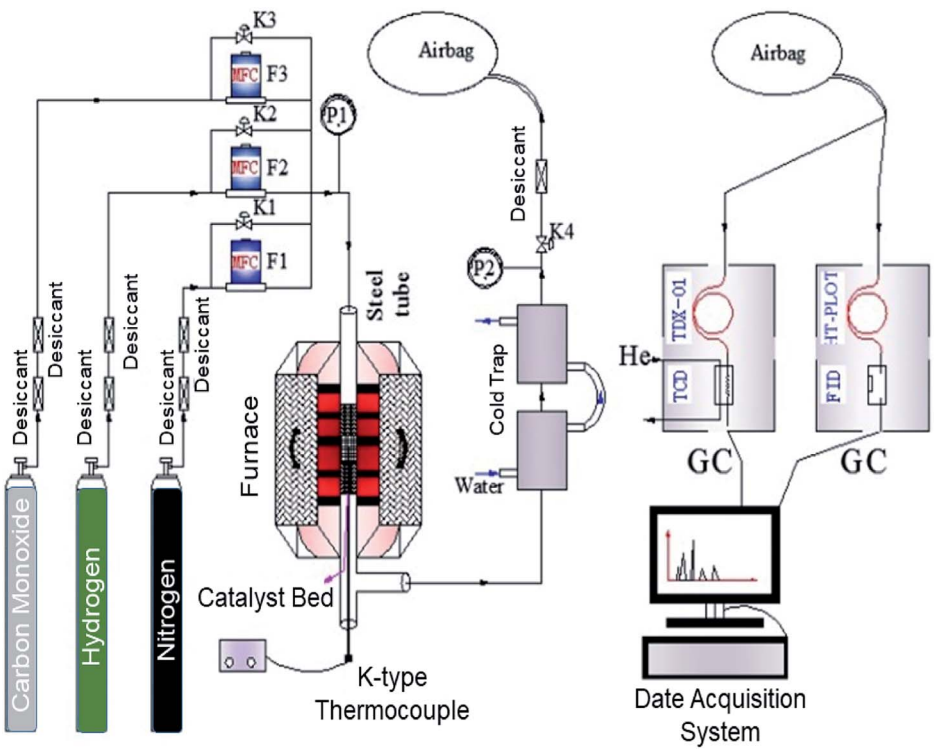

Fig. 2 Schematic illustrating the flow chart of the apparatus for FTS reaction process.

C_2H_6, C_3H_6, C_3H_8, C_4H_8, C_4H_{10}, C_5^+) were calculated with detected experimental data. Prior to the experiment, the peak areas of C_2H_4, C_2H_6, C_3H_6, C_3H_8, C_4H_8, and C_4H_{10}, were corrected by standard gas (N_2 3.0%, CH_4 5.4%, C_2H_4 15.4%, C_2H_6 15.5%, C_3H_6 15.1%, C_3H_8 15.7%, C_4H_8 14.9%, and C_4H_{10} 15.0%). Moreover, the correction factor of CO_2 was set as $f_{CO_2} = 1$. In addition, the relative correction factors ($f^*_{C_2H_6} = 0.819, f^*_{C_2H_4} = 0.817, f^*_{C_3H_8} = 0.537, f^*_{C_3H_6} = 0.535, f^*_{C_4H_{10}} = 0.397$, and $f^*_{C_4H_8} = 0.432$) were obtained. Eventually, the conversion of CO and H_2, selectivity of CO_2, and hydrocarbon were calculated according to the following formulae:

$$C_{CO} = \frac{n^{in}_{CO} - n^{out}_{CO}}{n^{in}_{CO}} = 1 - \frac{A^{out}_{CO}A^{in}_{N_2}}{A^{in}_{CO}A^{out}_{N_2}} \quad (1)$$

$$C_{H_2} = \frac{n^{in}_{H_2} - n^{out}_{H_2}}{n^{in}_{H_2}} = 1 - \frac{A^{out}_{H_2}A^{in}_{N_2}}{A^{in}_{H_2}A^{out}_{N_2}} \quad (2)$$

$$S_{CO_2} = \frac{n^{out}_{CO_2} - n^{in}_{CO_2}}{n^{in}_{CO} - n^{out}_{CO}} = \frac{f_{CO_2}\left(A^{out}_{CO_2}A^{in}_{N_2} - A^{in}_{CO_2}A^{out}_{N_2}\right)}{f^*_{CO}\left(A^{in}_{CO}A^{out}_{N_2} - A^{out}_{CO}A^{in}_{N_2}\right)} \quad (3)$$

$$S_{CH_4} = \frac{n^{out}_{CH_4} - n^{in}_{CH_4}}{n^{in}_{CO} - n^{out}_{CO}} = \frac{f^*_{CH_4}\left(A^{out}_{CH_4}A^{in}_{N_2} - A^{in}_{CH_4}A^{out}_{N_2}\right)}{f^*_{CO}\left(A^{in}_{CO}A^{out}_{N_2} - A^{out}_{CO}A^{in}_{N_2}\right)} \quad (4)$$

$$S_i = \frac{n^{out}_i - n^{in}_i}{n^{in}_{CO} - n^{out}_{CO}} = \frac{S_{CH_4}f^*_i\left(A^{out}_i - A^{in}_i\right)}{f^*_{CH_4}\left(A^{out}_{CH_4} - A^{in}_{CH_4}\right)} \quad (5)$$

$$S_{C_5^+} = 1 - S_i (I \leq 4) \quad (6)$$

where A^{out}_x (x = H_2, N_2, CO, CO_2, CH_4, C_2H_4, C_2H_6, C_3H_6, C_3H_8, C_4H_8, C_4H_{10}, and C_5^+) represents the GC peak area of the corresponding tail gas; A^{in}_x (x = H_2, N_2, CO, CO_2, CH_4, C_2H_4, C_2H_6, C_3H_6, C_3H_8, C_4H_8, C_4H_{10}, and C_5^+) represents the GC peak area of the corresponding reaction gas.

Result and discussions

Characterization of the catalysts

Iron carbides consist of carbon atoms occupying the interstices between close-packed iron atoms, and they can be further classified according to whether the carbon atoms are located in trigonal-prismatic interstices (Fe_3C, Fe_5C_2, and Fe_7C_3) or octahedral interstices ($Fe_{2.2}C$ and Fe_2C). In particular, Hägg iron carbide (Fe_5C_2) has a monoclinic unit cell with space group $C2/c$ (a = 11.5620 Å, b = 4.5727 Å, c = 5.0595 Å, and β = 97.74°).[26] Crystallite structures of the prepared Fe_5C_2 particles were examined by XRD and the results are shown in Fig. 3(a). Comparatively, the two Fe_5C_2@ZSM-5 catalysts prepared by different methods had not shown the diffraction peaks of hematite (α-Fe_2O_3), but the obvious diffraction peaks of Fe_5C_2 could represent at 2θ values of 43.4° and 44.1°. The tiny difference of Fe_5C_2@ZSM-5 catalysts prepared by two methods indicated that the order of coating and carbonization had no obvious effect on the formation of Fe_5C_2.

Fig. 3(c) depicts the XRD patterns of Fe_5C_2@ZSM-5 catalysts with different amounts of ZSM-5 molecular sieves. It was explicitly observed that with the increase in the coating amount

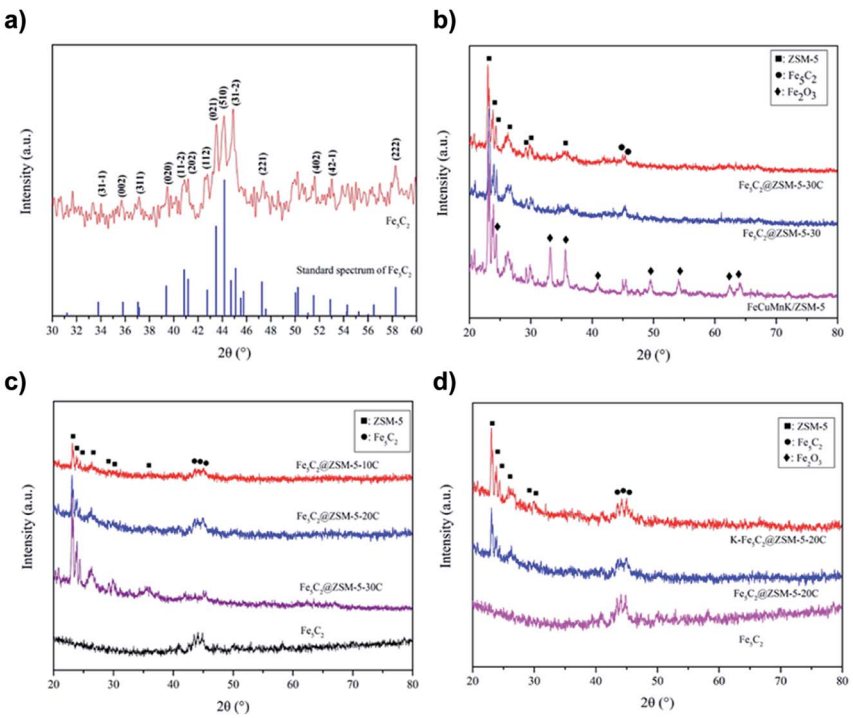

Fig. 3 XRD patterns of different catalysts and precursors, (a) Fe_5C_2 particles, (b) different Fe-based catalysts, (c) Fe_5C_2@ZSM-5 catalysts with the different coating amounts of ZSM-5, and (d) K–Fe_5C_2@ZSM-5 catalysts.

Table 1 Textural properties of different Fe-based catalysts

Catalysts	Surface area ($m^2\ g^{-1}$)	Pore volume ($cm^3\ g^{-1}$)	Pore size (nm)
Fe_5C_2@ZSM-5-30C	210.1	0.26	4.98
Fe_5C_2@ZSM-5-30	196.2	0.37	7.51
K–Fe/ZSM-5	174.6	0.13	3.01

Table 2 Textural properties of different core–shell catalysts

Catalysts	Surface area ($m^2\ g^{-1}$)	Pore volume ($cm^3\ g^{-1}$)	Pore size (nm)
Fe_5C_2@ZSM-5-10C	101.3	0.13	6.33
Fe_5C_2@ZSM-5-20C	118.7	0.16	5.72
Fe_5C_2@ZSM-5-30C	210.1	0.26	4.98
K–Fe_5C_2@ZSM-5-20C	126.5	0.17	5.17

of molecular sieve, the intensity of characteristic diffraction peak of the molecular sieve ZSM-5 (JCPDS card no. 44-0003), was increased, while the intensity of the characteristic diffraction peak of Fe_5C_2 was weakened. The XRD pattern of the K–Fe_5C_2@ZSM-5-20C catalysts by adding the K^+ promoter is shown in Fig. 3(d). Further, no characteristic diffraction peak of K^+ was evident in the spectrum, indicating that K^+ does not change the structural of catalysts. It was consistent with the research results of Visconti *et al.*[27] Temperature-programmed desorption(TPD) were carried out from 100 °C to 550 °C at a heating rate of 10 °C min^{-1} using helium as the carrier gas. The results showed the NH_3 desorption peaks for ZSM-5 zeolite mainly located at about 250 °C, attributed to the weak acid sites on Si–O–Si units and some physical ammonia adsorption. A little difference between K–Fe_5C_2@ZSM-5 and Fe_5C_2@ZSM-5 except for a slight low-temperature shift of NH_3 desorption peak on K–Fe_5C_2@ZSM-5. It is believed acid strength in the acid centers of K–Fe_5C_2@ZSM-5 was reduced, because acid centers in the surface of catalyst might be neutralized.

BET results

The surface area, total pore volume, and pore size of different iron-based catalysts for FTS are summarized in Table 1. The surface area, total pore volume, and pore size of K–Fe/ZSM-5 catalyst, prepared by the conventional impregnation method, were much lower than those of core–shell Fe_5C_2@ZSM-5 catalysts. From Table 1, it was obvious that the specific surface area of Fe_5C_2@ZSM-5-30C catalysts was higher than that of Fe_5C_2@ZSM-5-30 catalysts, while the total pore volume and pore size were smaller than that of Fe_5C_2@ZSM-5-30 catalysts. These advantages of Fe_5C_2@ZSM-5-30C catalyst could be helpful to provide more active sites and to better screen high carbon chain hydrocarbons, which could be beneficial in improving the selectivity of low carbon hydrocarbons.[28]

The BET data of different coating amounts of ZSM-5 molecular sieve and K^+ doped Fe_5C_2@ZSM-5 catalysts are shown in Table 2. It was observed from the experimental results that the specific surface area and total pore volume of Fe_5C_2@ZSM-5 catalysts were gradually increased with the increase in the coating amount of ZSM-5 molecular sieve, attributed to the porosity provided by coating amount of ZSM-5 molecular sieve. Further, the decrease in the pore size as the increase of ZSM-5 molecular sieve implied that more amount of ZSM-5 molecular sieve was coated on the catalyst shell. Notably, the modification of the K^+ promoter has no effect on the porous structures and specific surface area of the catalysts, as presented in Table 2.

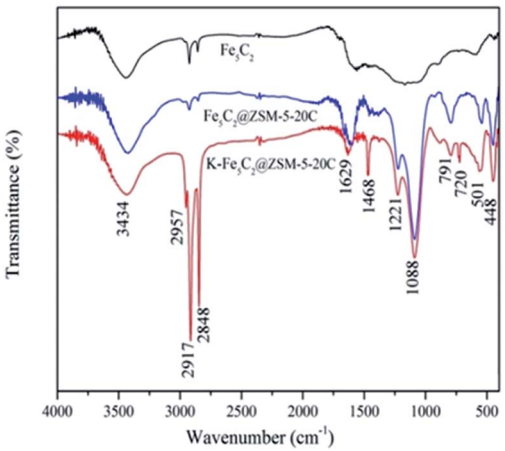

Fig. 4 FT-IR spectra of Fe_5C_2, Fe_5C_2@ZSM-5-20C, and K–Fe_5C_2@ZSM-5-20C catalysts.

FT-IR recordings

Further, FT-IR profiles of Fe_5C_2, Fe_5C_2@ZSM-20C, and K–Fe_5C_2@ZSM-20C catalysts were recorded, as presented in Fig. 4. The absorption peaks near 3434 cm^{-1} could be attributed to O–H stretching vibration of –OH, and the peak at 1629 cm^{-1} could be ascribed to the adsorption peak of physisorbed water on the surface of the catalyst.[29] Further, the characteristic peaks at 2848 and 2917 cm^{-1}, could correspond to Fe_5C_2. Notably, these characteristic peaks of Fe_5C_2 were weakened after coated with ZSM-5 (Fe_5C_2@ZSM-20C), while several characteristic absorption peaks of ZSM-5 zeolite could be represented in the range of 400–1300 cm^{-1}. Within the fingerprint region of IR, the peaks appearing at 501, 448, and 791 cm^{-1} could be assigned to the absorption peak of the ZSM-5 five-membered ring, the variable angle vibration absorption peak caused by Al–O bond, the Si–O bond, and the framework vibration of ZSM-5 zeolite, respectively. However, the characteristic absorption peaks of Fe_5C_2 increased significantly, and new absorption peaks at 720, 1468, and 2957 cm^{-1} have appeared after K doped into Fe_5C_2@ZSM-20C catalyst.[30]

FE-SEM observations

FE-SEM images of Fe_5C_2@ZSM-5 catalysts with different ZSM-5 molecular sieves are depicted in Fig. 5. It was observed from the experimental results that the Fe_5C_2 particles representing the core of the catalyst were irregular micro-sized particles with a diameter of about 1 μm, while the ZSM-5 zeolite particles, the

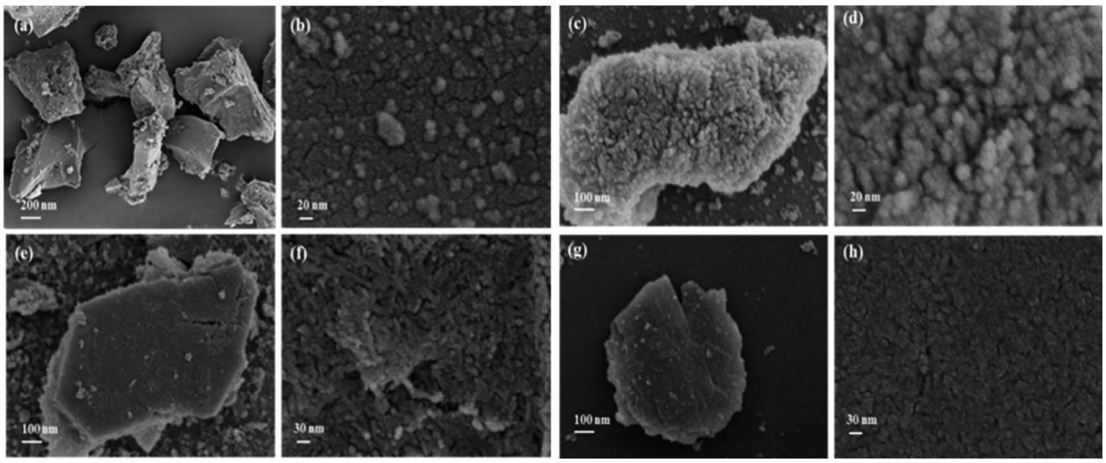

Fig. 5 FE-SEM micrographs of Fe_5C_2@ZSM-5 catalysts with different coating amounts of ZSM-5. (a) Fe_5C_2 particles, (b) ZSM-5 particles(c) Fe_5C_2@ZSM-5-10C, (d) the partial enlarged view of Fe_5C_2@ZSM-5-10C, (e) Fe_5C_2@ZSM-5-20C, (f) the partial enlarged view of Fe_5C_2@ZSM-5-20C, (g) Fe_5C_2@ZSM-5-30C, (h) the partial enlarged view of Fe_5C_2@ZSM-5-30C.

shell of catalyst, were nano-sized particles with a diameter of about 20 nm (Fig. 5(a and b)). To this end, the core–shell Fe_5C_2@ZSM-5 catalyst particles prepared by coating after carbonization were obtained without collapse and fracture, indicating that the iron oxide core during the carbonization process had no substantial effect on the integrity of the shell (Fig. 5(c–h)). However, the texture of the shell surface of the catalysts was changed to smooth with the increase of the ZSM-5 coating amount. Moreover, the gap between the particles became smaller gradually, from about 10 nm to almost no gap with the increase of the ZSM-5 coating amount. In an instance of the ZSM-5 coating amount increased from 10 wt% to 20 wt%, the fine particles adhered to the surface of the catalyst were changed from the spherical shape with a diameter of 20 nm to rod-like architectures with a diameter of 50–100 nm. Further, an increase in the coating amount to 30 wt%, the ZSM-5 zeolites were closely arranged and thus occurred the phenomenon of serious agglomeration. Together, it could be elucidated that the Fe_5C_2 active component could be coated by the nano-sized ZSM-5 molecular sieve particles by the coating method. With the increase in the coating amount of ZSM-5 molecular sieve, the surface of the catalyst particles was smooth, and the pore structure of the catalyst surface was also dense.

TEM observations

Fig. 6 depicts the TEM images of K–Fe_5C_2@ZSM-5-20C catalyst, Fe_5C_2, and ZSM-5 molecular sieves. In Fig. 6(a), the prepared K-doped Fe_5C_2 particles were irregular micron-sized particles with good crystallinity. Moreover, the average size of ZSM-5 zeolite particles was 20 nm in diameter and showed a good dispersibility (Fig. 6(b)). The TEM image of core–shell K–Fe_5C_2@-ZSM-5-20C catalyst particles is shown in Fig. 6(c). It was observed that the fabricated core–shell structures were irregular in shape, and the core K-doped Fe_5C_2 particles were bonded by granular ZSM-5 zeolites shell. The catalyst was irregular micro-sized particles with 1 μm in diameter, and the thickness of the shell was not uniform in the ranges of 200–500 nm. Notably, no obvious collapse or deformation in K–Fe_5C_2@ZSM-5-20C of core Fe_5C_2 was observed, while the outer layer of ZSM-5 zeolites was bond to the core. Therefore, it could be believed that the

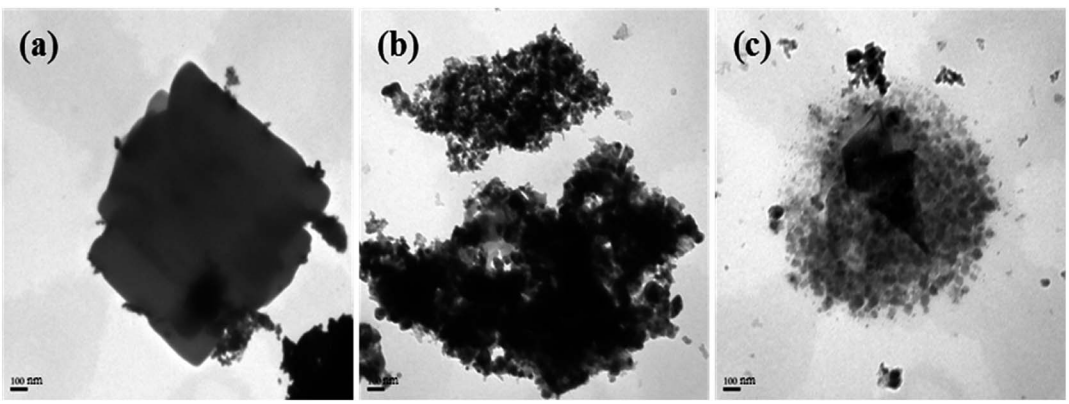

Fig. 6 TEM micrographs of Fe_5C_2 particles, ZSM-5 particles, and K–Fe_5C_2@ZSM-5-20C. (a) K–Fe_5C_2 particles, (b) ZSM-5 particles, (c) K–Fe_5C_2@ZSM-5-20C.

Table 3 The CO conversion and light olefins distribution over different Fe-based catalysts[a]

Catalysts	$C_{(CO)}$ (%)	$S_{(CO_2)}$ (%)	Selective distribution of low carbon hydrocarbons (%)							
			CH_4	C_2H_4	C_3H_6	C_4H_8	C_2–C_4	C_5^+	C_2–$C_4^=$	O/P
Fe_5C_2@ZSM-5-30C	42.58	23.18	28.45	9.29	6.88	6.67	16.71	31.99	22.85	1.37
Fe_5C_2@ZSM-5-30	49.02	26.67	31.58	8.64	8.08	5.75	10.90	35.04	22.47	2.06
K–Fe/ZSM-5	32.75	26.41	24.75	2.82	0.90	1.26	4.34	65.92	4.98	1.15

[a] C2–C4 = represents C2–C4 olefins. O/P is the ratio of olefins to alkanes in the outcome.

Table 4 The CO conversion and light olefins distribution over Fe_5C_2@ZSM-5 catalysts with the different coating amounts of ZSM-5[a]

Catalysts	$C_{(CO)}$ (%)	$S_{(CO_2)}$ (%)	Selective distribution of low carbon hydrocarbons (%)							
			CH_4	C_2H_4	C_3H_6	C_4H_8	C_2–C_4	C_5^+	C_2–$C_4^=$	O/P
Fe_5C_2	62.45	28.52	14.37	2.06	3.11	2.03	4.64	73.79	7.20	1.55
Fe_5C_2@ZSM-5-10C	56.50	26.41	17.98	2.82	3.90	2.26	6.34	66.70	8.98	1.42
Fe_5C_2@ZSM-5-20C	47.47	24.11	24.77	12.75	9.10	7.24	13.40	32.74	29.09	2.17
Fe_5C_2@ZSM-5-30C	49.02	26.67	31.58	8.64	8.08	5.75	10.90	35.04	22.47	2.06
K–Fe_5C_2@ZSM-5-20C	53.75	20.20	19.76	13.55	11.58	12.13	14.86	28.12	37.25	2.51

[a] C_2–$C_4^=$ represents C_2–C_4 olefins. O/P is the ratio of olefins to alkanes in the outcome.

method of carbonization after coating was feasible to prepare the core–shell K–Fe_5C_2@ZSM-5-20C catalyst.

FTS performance of core–shell catalysts

The FTS performance efficacy of the core–shell Fe_5C_2@ZSM-5 catalyst was compared with the supported K–Fe/ZSM-5 catalyst. The effects of the order of coating and carbonization on the core–shell Fe_5C_2@ZSM-5 catalyst were mainly analyzed. Table 3 shows the conversion of CO and the distribution of low carbon olefins on different iron-based catalysts. In Table 3, the CO conversion and the selectivity of low carbon olefins and low carbon alkanes of K–Fe/ZSM-5 catalyst were much lower than those of Fe_5C_2@ZSM-5 catalyst, but the selectivity of C_5^+ component was much higher, indicating that the breaching effect of core–shell Fe_5C_2@ZSM-5 catalyst on high carbon hydrocarbons resulted in more low carbon hydrocarbons, and thus increased the selectivity of low carbon olefins. The CO conversion and selectivity of CO and CH_4 on Fe_5C_2@ZSM-5-30C catalyst were slightly higher than those on Fe_5C_2@ZSM-5-30 catalyst, while C_5^+ component selectivity of both catalysts was below 35%. In regard to the distribution of low olefins, C2–C4 olefins (C_2–$C_4^=$) selectivity on both of core–shell Fe_5C_2@ZSM-5 catalysts were about 22% while the O/P ratio of olefins to alkanes of Fe_5C_2@ZSM-5-30C catalyst was higher than that of Fe_5C_2@ZSM-5-30 catalyst. Fig. 3 shows that the order of coating and carbonization has little effect on the core–shell structure of Fe_5C_2@ZSM-5 catalysts, but the results of FTS experiments implied that the preparation method of carbonization after coating was beneficial in improving the selectivity of low carbon olefins. To further explore the effects of ZSM-5 zeolite and K^+ doping on the performance of Fe_5C_2@ZSM-5 catalysts in FTS, the Fe_5C_2@ZSM-5 catalysts with different zeolite coating amounts and K^+ doping Fe_5C_2@ZSM-5 with 20 wt% of zeolites were employed in FTS.

The CO conversion and low carbon hydrocarbons distribution on Fe_5C_2@ZSM-5 catalysts with different molecular sieve coating amounts in FTS are summarized in Table 4. It was observed that the Fe_5C_2 particles without the ZSM-5 zeolite exhibited the highest CO conversion and the highest selectivity for C_5^+ components, but the selectivity of low carbon olefins was the lowest. These consequences implied that iron carbide particles were highly reactive in FTS, while high carbon hydrocarbons were favorable to be generated on iron carbides. Molecular sieve could act as a well catalytic cracking catalyst because of its controllable pore structure and adjustable acidity. Herein, the ZSM-5 zeolites were designed as the shell of the Fe_5C_2@ZSM-5 catalyst, which was expected to play two roles in FTS. In this vein, one of the roles was the screening of the low carbon hydrocarbons from the products generated on the iron carbide active centre (preventing from the export of long-chain hydrocarbons), while the other was catalytic cracking of the long-chain hydrocarbons into low carbon olefins.

Table 4 demonstrates that the selectivity of CH_4, C_2H_4, C_3H_6, C_4H_8, and C_2–$C_4^=$ as well as the ratio of O/P, which were significantly increased by coating ZSM-5 on Fe_5C_2. However, the conversion of CO was decreased (derived from the decrease of the relative percentage of active component iron carbides). In addition, while the coating amount of ZSM-5 zeolite was 10 wt%, the selectivity of low carbon hydrocarbons was higher than that of the Fe_5C_2 catalyst. It should be noted that it was much lower than that of 20 wt% and 30 wt%, while the selectivity of C_5^+ was much higher than that of both. When the coating amount of ZSM-5 zeolite was 20 wt%, the Fe_5C_2@ZSM-5-20C catalyst had shown the lowest CO conversion, the highest

Table 5 Catalytic performance on promoted iron F–T catalysts in published references

Catalyst	Temp (°C)	Press (MPa)	H_2/CO	CO conv. (%)	Sel. in hydrocarbons/wt%				CO_2 sel. (%)	O/P ratio[a]	Ref.
					CH_4	C_2–C_4	C_5–C_{11}	C_{12}^+			
Fe–Cu-1.5K/SiO_2	280	0.2	2.0	2.12	23	77	7[b]		67	10.1	33
Fe-5% K/SiO_2	230	1.2	0.67	38	1.4	28.6	31.3	38.7	38	6.1	34
Fe–K–Mo5-1/SiO_2	280	1.5	1.2	27.8	8.8	21.7	38.1	31.5	33.3	1.95	35
Fe–Zn–K_4–Cu_2	200	2.0	2.0	50	2.0	8.9	89.1[b]		15.8	NA	36
Fe–Mn–Cu–K/SiO_2	270	1.5	0.67	62.1	8.2	23.7	41.8	24.1	NA	1.9	37
Fe-0.1% Pd/MgO	300	0.5	2.0	6.8	67	19	14		NA	1.4	38

[a] Olefin to paraffin weight ratios for C_2–C_4. [b] Data represent C_5^+ hydrocarbons selectivity. NA, data not available; carbon selectivity is defined as the carbon atoms in the total number of C atoms in hydrocarbon products, CO_2 is not included. Some values are recalculated from the original data reported in literature.

selectivity of low carbon olefins and alkanes, and the highest O/P ratio. However, the difference between the catalysts with the coating amount of ZSM-5 20 wt% and 30 wt% was not significant, implying that the thickness of the molecular sieve shell exited an optimum value. Probably, it might be linked to the degree of catalytic break down of long-chain products.

Previous reports indicated that slight alkali metal added into iron carbides favoured receding the electron affinity of iron,[31] and the adsorption of hydrogen on iron,[32] resulting in the decrease of hydrogenation activity of iron carbide catalyst and the increase of adsorption of CO on active iron centre. In this context, the addition of potassium had significantly augmented the surface area and dispersity of iron phase in catalysts, enhancing the metal-support interaction, and restraining the phase transformation, and coking of iron-base catalyst. In Table 4, the data showed that slight potassium in catalysts helped in increasing the catalytic activity and selectivity. Further, the CO conversion, the ratio of O/P, and the selectivity of ethylene, propylene, butene, and C_2–$C_4^=$ on K–Fe_5C_2@ZSM-20C catalyst were significantly improved. The K-doping catalyst showed the highest selectivity of four to five carbons alkene with 37.25% and the highest ratio of olefins to alkanes in the outcome. The selectivity of CO_2, CH_4, and C_5^+ was decreased, compared to that of Fe_5C_2@ZSM-20C, while the CO conversion on K–Fe_5C_2@ZSM-20C still remained well. A lot of related papers were reviewed and the catalytic results were summarized in Table 5 below. From the comparison of Table 4 in our manuscript and Table 5, it is found the reported Fe-catalysts with different promoters, as a whole, show lower conversion of CO and higher selectivity of CO_2 than our catalyst K–Fe_5C_2@ZSM-5-20C. Moreover, the sum of selectivity of low carbon hydrocarbons (C_2H_4, C_3H_6, C_4H_8, C_2–C_4) in Table 4 is 52%, much higher than that in Table 5. It indicates that the prepared K–Fe_5C_2@ZSM-5-20C had a well selectivity of low carbon hydrocarbons which are considered as value platform chemical compounds. Therefore, it can be believed our catalyst is successful in improving the conversion of CO and selectivity of low carbon hydrocarbons.

As a summary of the characterization of K–Fe_5C_2@ZSM-5-20C, K doping was beneficial to enhance the activity of Fe_5C_2 components of the catalyst and increase the pore structure and specific surface area of the catalyst and the screening effect of high carbon number hydrocarbons in products. Combining the characterization with the results of FTS, we believe that the K doping had significantly improved the reactive activity of core–shell Fe_5C_2@ZSM-5 catalyst and selectivity of low carbon olefins.

Conclusions

Low carbon olefins, such as ethylene and propylene, are extensive and prosperous platform chemical compounds. FTS is a well-known good way to get low carbon olefins from CO or CO_2. However, the key factor is to prepare the highly active and selective catalyst. In this approach, the catalyst, iron carbide, acted as an active centre for CO hydrogenation to provide an active iron centre for the FTS reaction, and Fe_5C_2 was the final active phase of iron-based catalyst. Molecular sieve played a role in catalytic cracking catalyst because of its controllable pore structure and adjustable acidity. Here, a core–shell FTS catalyst (ZSM-5 capped Fe_5C_2) was designed and prepared by the coating-carbonization method. ZSM-5 zeolites were used to screen the low carbon hydrocarbons from the products generated on the iron carbide active centre (preventing from the export of long-chain hydrocarbons), and to break down the long-chain hydrocarbons into low carbon olefins catalytically. These results manifested that the core–shell Fe_5C_2@ZSM-5 catalysts had higher CO conversion rate, reaction activity, and selectivity of low-carbon olefins, compared to a K–Fe/ZSM-5 prepared by traditional impregnation method. Comparatively, the Fe_5C_2@ZSM-5C catalyst prepared by carbonization after coating method exhibited more surface area, smaller average pore size, and more reactive active sites, resulting in the improvement of screening high carbon hydrocarbons and the enhancement of selectivity to low carbon olefins, than those of prepared by coating after carbonization method. The optimal coating amount of ZSM-5 was about 20 wt%. Another advantage is that the K-doping catalyst showed the highest selectivity of two to four carbons alkene with 37.25% and the highest ratio of olefins to alkanes in the outcome, while the CO conversion on K–Fe_5C_2@ZSM-20C still remained well. Together, our findings showed that the core–shell Fe_5C_2@ZSM-5 catalyst had shown

significantly improved the reactivity as well as the selectivity of low carbon olefins.

Conflicts of interest

There are no conflicts to declare.

Acknowledgements

This work was financially supported by the Xiamen science and technology project foundation (Grant No. 3502Z20183024), the National Natural Science Foundation of China (Grant No. 21603077 and 51603077), and Postgraduates' Innovative Fund in Scientific Research of Huaqiao University.

Notes and references

1 M. E. Dry, *Catal. Today*, 2002, **71**, 227–241.
2 C. Wei, B. Zijlstra, R. Pestman and E. Hensen, *ChemCatChem*, 2018, **10**, 136–140.
3 W. Chen, T. Lin, Y. Dai, Y. An, F. Yu, L. Zhong, S. Li and Y. Sun, *Catal. Today*, 2018, **311**, 8–22.
4 A. P. Steynberg, Introduction to Fischer-Tropsch Technology Studies, in *Surface Science and Catalysis*, ed. A. P. Steynberg and M. Dry, 2004, vol. 152, pp. 1–63.
5 A. A. Vasilev, M. N. Efimov, G. N. Bondarenko, D. G. Muratov, E. L. Dzidziguri, M. I. Ivantsov, M. V. Kulikova and G. P. Karpacheva, *Chem. Phys. Lett.*, 2019, **730**, 8–13.
6 J. van de Loosdrecht, F. G. Botes, I. M. Ciobica, A. Ferreira, P. Gibson, D. J. Moodley, A. M. Saib, J. L. Visagie, C. J. Weststrate and J. W. Niemantsverdriet, Fischer–Tropsch Synthesis: Catalysts and Chemistry, in *Comprehensive Inorganic Chemistry II*, ed. J. Reedijk and K. Poeppelmeier, 2013, vol. 7, pp. 525–557.
7 X. Zhao, S. Lv, L. Wang, L. Li, G. Wang, Y. Zhang and J. Li, *Mol. Catal.*, 2018, **449**, 99–105.
8 Y. Wang, Y. Li, S. Huang, J. Wang, H. Wang, J. Lv and X. Ma, *Chem. Phys. Lett.*, 2017, **682**, 115–121.
9 J. Li, Y. Hou, Z. Song, C. Liu, W. Dong, C. Zhang, Y. Yang and Y. Li, *Mol. Catal.*, 2018, **449**, 1–7.
10 J. Tu, M. Ding, T. Wang, L. Ma, Y. Xu, S. Kang and G. Zhang, *Energy Procedia*, 2017, **105**, 82–87.
11 M. Zhang, J. Ren and Y. Yu, *ACS Catal.*, 2020, **10**, 689–701.
12 T. A. Wezendonk, X. Sun, A. Iulian Dugulan, A. J. F. van Hoof, E. J. M. Hensen, F. Kapteijn and J. Gascon, *J. Catal.*, 2018, **362**, 106–117.
13 D. Peña, A. Cognigni, T. Neumayer, W. van Beek, D. S. Jones, M. Quijada and M. Rønning, *Appl. Catal., A*, 2018, **554**, 10–23.
14 L. Tang, X. L. Dong, W. Xu, L. He and A. H. Lu, *Chin. J. Catal.*, 2018, **39**, 1971–1979.
15 D. Wang, B. Chen, X. Duan, D. Chen and X. Zhou, *J. Energy Chem.*, 2016, **25**, 911–916.
16 J. G. Rivera de la Cruz, M. K. Sabbe and M. F. Reyniers, *Mol. Catal.*, 2018, **453**, 55–63.
17 N. E. Tsakoumis, M. Rønning, Ø. Borg, E. Rytter and A. Holmen, *Catal. Today*, 2010, **154**, 162–182.
18 R. A. Dictor and A. T. Bell, *J. Catal.*, 1986, **97**, 121–136.
19 J. Li, X. Cheng, C. Zhang, Q. Chang, J. Wang, X. Wang, Z. Lv, W. Dong, Y. Yang and Y. Li, *Appl. Catal., A*, 2016, **528**, 131–141.
20 Y. Cheng, M. Qiao and B. Zong, Fischer–Tropsch Synthesis, in *Encyclopedia of Sustainable Technologies*, ed. M. A. Abraham, 2017, vol. 3, pp. 403–410.
21 M. O. Ozbek and J. W. Niemantsverdriet, *J. Catal.*, 2014, **317**, 158–166.
22 W. Ma, G. Jacobs, V. R. R. Pendyala, D. E. Sparks, W. D. Shafer, G. A. Thomas, A. MacLennan, Y. Hu and B. H. Davis, *Catal. Today*, 2018, **299**, 28–36.
23 X. Wen, Y. H. Zhang, C. C. Liu, J. Hong, L. Wei, Y. Chen and J. L. Li, *J. Fuel Chem. Technol.*, 2017, **45**, 950–955.
24 D. Wu and M. Tang, *Powder Technol.*, 2019, **352**, 79–90.
25 O. Ben Moussa, I. Borghol, D. Hu, S. Casale, Y. Millot, C. Sayag, J. Blanchard and O. Durupthy, *Microporous Mesoporous Mater.*, 2019, **287**, 177–182.
26 X. Liu, S. Zhao and Y. Meng, *Sci. Rep.*, 2016, **26184**, 1–10.
27 C. G. Visconti, M. Martinelli, L. Falbo and A. I. Molina, *Appl. Catal., B*, 2016, **200**, 530–542.
28 K. Cheng, M. Virginie, V. V. Ordomsky, C. Cordier, P. A. Chernavskii, M. I. Ivantsov, S. Paul, Y. Wang and A. Y. Khodakov, *J. Catal.*, 2015, **328**, 139–150.
29 R. A. V. Santen, A. J. Markvoort, I. A. W. Filot, M. M. Ghouri and E. J. M. Hensen, *Phys. Chem. Chem. Phys.*, 2013, **15**, 17038–17063.
30 G. Yu, B. Sun, Y. Pei, S. Xie, S. Yan, M. Qiao, K. Fan, X. Zhang and B. Zong, *J. Am. Chem. Soc.*, 2010, **132**, 935–937.
31 A. Dinse, M. Aigner, M. Ulbrich, G. R. Johnson and A. T. Bell, *J. Catal.*, 2012, **288**, 104–114.
32 C. Qin and J. Li, *Catal. Commun.*, 2008, **9**, 2003–2006.
33 N. Lohitharn and J. G. Goodwin, *J. Catal.*, 2008, **260**, 7–16.
34 M. S. Luo, R. J. O'Brien, S. Q. Bao and B. H. Davis, *Appl. Catal., A*, 2003, **239**, 111–120.
35 S. D. Qin, C. H. Zhang, J. Xu, B. S. Wu, H. W. Xiang and Y. W. Li, *J. Mol. Catal. Chem.*, 2009, **304**, 128–134.
36 S. Z. Li, S. Krishnamoorthy, A. W. Li, G. D. Meitzner and E. Iglesia, *J. Catal.*, 2002, **206**, 202–217.
37 C. H. Zhang, Y. Yang, B. T. Teng, T. Z. Li, H. Y. Zheng, H. W. Xiang and Y. W. Li, *J. Catal.*, 2006, **237**, 405–415.
38 M. Minnermann, S. Pokhrel, K. Thiel, R. Henkel and J. Birkenstock, *J. Phys. Chem. C*, 2011, **115**, 1302–1310.